

Thermoelectric properties of orthorhombic group IV-VI monolayers from the first-principles calculations

San-Dong Guo

Department of Physics, School of Sciences, China University of Mining and Technology, Xuzhou 221116, Jiangsu, China

Two-dimensional (2D) materials may have potential applications in thermoelectric devices. In this work, we systematically investigate the thermoelectric properties of orthorhombic group IV-VI monolayers AB (A=Ge and Sn; B=S and Se) by the first-principles calculations and semiclassical Boltzmann transport theory. The spin-orbit coupling (SOC) is included to investigate their electronic transport, which produces observable effects on power factor, especially for n-type doping. According to calculated ZT , the four monolayers exhibit diverse anisotropic thermoelectric properties, although they have similar hinge-like crystal structure. The GeS along zigzag and armchair directions shows the strongest anisotropy, while SnS and SnSe show mostly isotropic efficiency of thermoelectric conversion, which can be understood by the strength of anisotropy of their respective power factor, electronic and lattice thermal conductivities. Calculated results show that ZT for different carriers of n- and p-type has little difference for GeS, SnS and SnSe. It is found that GeSe, SnS and SnSe show better thermoelectric performance compared to GeS in n-type doping, and SnS and SnSe exhibit higher efficiency of thermoelectric conversion in p-type doping. Compared to a lot of 2D materials, orthorhombic group IV-VI monolayers AB (A=Ge and Sn; B=S and Se) may possess better thermoelectric performance due to higher power factor and lower thermal conductivity. Our work would be beneficial to further experimental study.

PACS numbers: 72.15.Jf, 71.20.-b, 71.70.Ej, 79.10.-n

Keywords: Group IV-VI monolayers; Spin-orbit coupling; Power factor; Thermal conductivity

I. INTRODUCTION

Thermoelectric materials, which can directly convert heat to electricity or vice versa and make essential contributions to energy crisis and global warming, have been a hot spot^{1,2}. The conversion efficiency of thermoelectric materials can be measured by the dimensionless figure of merit $ZT = S^2\sigma T/(\kappa_e + \kappa_L)$, in which S , σ , T , κ_e and κ_L are the Seebeck coefficient, electrical conductivity, absolute temperature, the electronic and lattice thermal conductivities, respectively. The high-performance thermoelectric materials require a high power factor ($S^2\sigma$) and a low thermal conductivity ($\kappa = \kappa_e + \kappa_L$), leading to large ZT value. Unfortunately, they are generally coupled with each other, and enhancing one can have the opposite effect on another. Due to simultaneously increasing power factor and decreasing thermal conductivity³, low-dimensional materials may have important potential advantages to improve efficiency of thermoelectric conversion, and a lot of works have focused on 2D materials, such as monolayer phosphorene, monolayer silicene and semiconducting transition-metal dichalcogenide monolayers⁴⁻¹⁰.

The bulk orthorhombic group IV-VI compounds AB (A=Ge and Sn; B=S and Se) with puckered (hinge-like) layered structure are promising candidates for high-efficient thermoelectric materials due to large Seebeck coefficients, high power factors and low thermal conductivities¹¹. Bulk SnSe is especially a robust thermoelectric material with an unprecedented ZT of 2.6 at 973 K along the b axis due to ultralow thermal conductivity^{12,13}. Like other layered materials, 2D SnSe has been recently synthesized^{14,15}, which is reported to

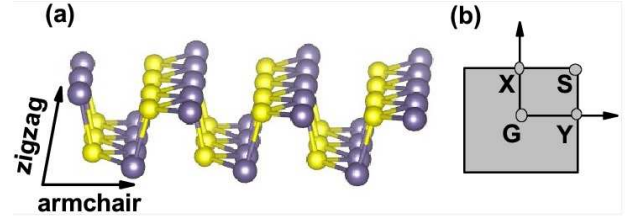


FIG. 1. (Color online) (a) The crystal structure of orthorhombic group IV-VI monolayers AB (A=Ge and Sn; B=S and Se); (b) the corresponding Brillouin-zone with the high symmetry points G, X, S and Y.

be a promising 2D semiconductor¹⁶, and the thermoelectric transport has been also investigated¹⁷. Besides 2D SnSe, the optical and piezoelectric properties of orthorhombic group IV-VI monolayers AB (A=Ge and Sn; B=S and Se) have been also studied¹⁸⁻²⁰. Moreover, it is predicted that orthorhombic group IV-VI monolayers are multiferroic with coupled ferroelectricity and ferroelasticity, and GeS and GeSe of them can maintain their ferroelasticity and ferroelectricity beyond the room temperature²¹. Recently, the phonon transport properties of orthorhombic group IV-VI monolayers have been systematically investigated by solving the Boltzmann transport equation (BTE) based on first-principles calculations, and they possess diverse anisotropic property of lattice thermal conductivity²². The average lattice thermal conductivities along the zigzag and armchair directions of group IV-VI monolayers are GeS ($6.38 \text{ Wm}^{-1}\text{K}^{-1}$), GeSe ($5.23 \text{ Wm}^{-1}\text{K}^{-1}$), SnS ($3.08 \text{ Wm}^{-1}\text{K}^{-1}$) and SnSe ($2.77 \text{ Wm}^{-1}\text{K}^{-1}$), which suggests that they may be potential 2D thermoelectric materials

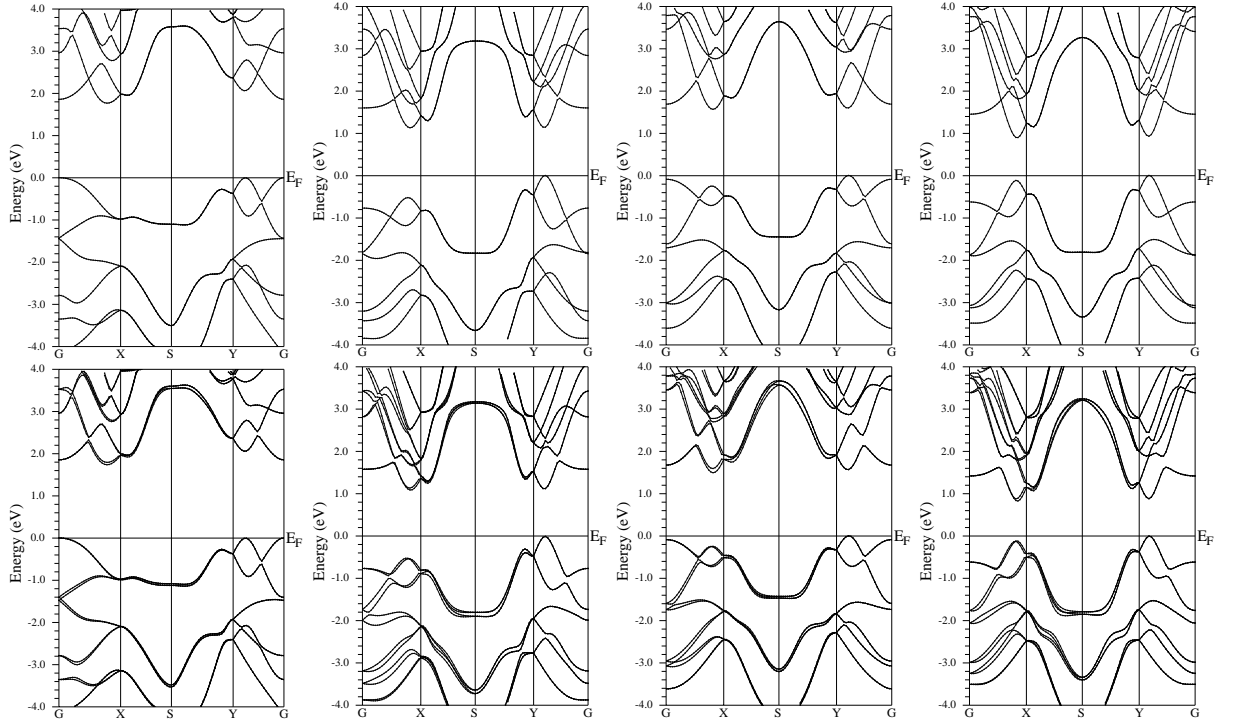


FIG. 2. The energy band structures of orthorhombic group IV-VI monolayers using GGA (Top) and GGA+SOC (Bottom). They from left to right are GeS, GeSe, SnS and SnSe, respectively.

due to rather low lattice thermal conductivity compared to other 2D materials.

TABLE I. The lattice constants²² a and b (Å) along zigzag and armchair directions; the calculated gap values using GGA G (eV) and GGA+SOC G_{so} (eV); $G-G_{so}$ (eV); spin-orbit splitting Δ_{so} (eV) at the CBM.

Name	a	b	G	G_{so}	$G-G_{so}$	Δ_{so}
GeS	3.671	4.457	1.767	1.736	0.031	0.057
GeSe	3.982	4.269	1.129	1.098	0.031	0.046
SnS	4.088	4.265	1.564	1.492	0.072	0.099
SnSe	4.294	4.370	0.895	0.829	0.066	0.052

Here, we report on the electronic structures and thermoelectric properties of orthorhombic group IV-VI monolayers AB (A=Ge and Sn; B=S and Se) from a combination of first-principles calculations and semiclassical Boltzmann transport theory. For electronic part, the SOC is included to attain reliable power factor and electronic thermal conductivity, which has been proved be very important for electron transport in many thermoelectric materials^{9,10,23–28}. It is found that SOC can produce observable influence on power factor in spite of little SOC effect on electronic structures, and the SOC not only can reduce power factor but it also can enhance one. The lattice thermal conductivities from Ref.²² and empirical scattering time $\tau=10^{-14}$ s are used to estimate dimensionless figure of merit ZT , which show that four

monolayers, although possessing similar hinge-like structure, show diverse anisotropic thermoelectric properties. The GeS shows the strongest anisotropy for ZT along the zigzag and armchair directions, while SnS and SnSe show neglectful anisotropy.

The rest of the paper is organized as follows. In the next section, we shall describe computational details for first-principle and transport coefficients calculations. In the third section, we shall present the electronic structures and thermoelectric properties of orthorhombic group IV-VI monolayers AB (A=Ge and Sn; B=S and Se). Finally, we shall give our discussions and conclusion in the fourth section.

II. COMPUTATIONAL DETAIL

A full-potential linearized augmented-plane-waves method within the density functional theory (DFT)²⁹ is employed to study electronic structures of orthorhombic group IV-VI monolayers AB (A=Ge and Sn; B=S and Se), as implemented in the WIEN2k package³⁰. The popular generalized gradient approximation (GGA)³¹ for the exchange-correlation potential is used to do our electronic structures calculations. The internal atomic position parameters are optimized using GGA with a force standard of 2 mRy/a.u.. The SOC was included self-consistently^{32–35} due to containing heavy elements, which leads to band splitting, giving rise to important influences on semi-classic transport coefficients. To attain accurate

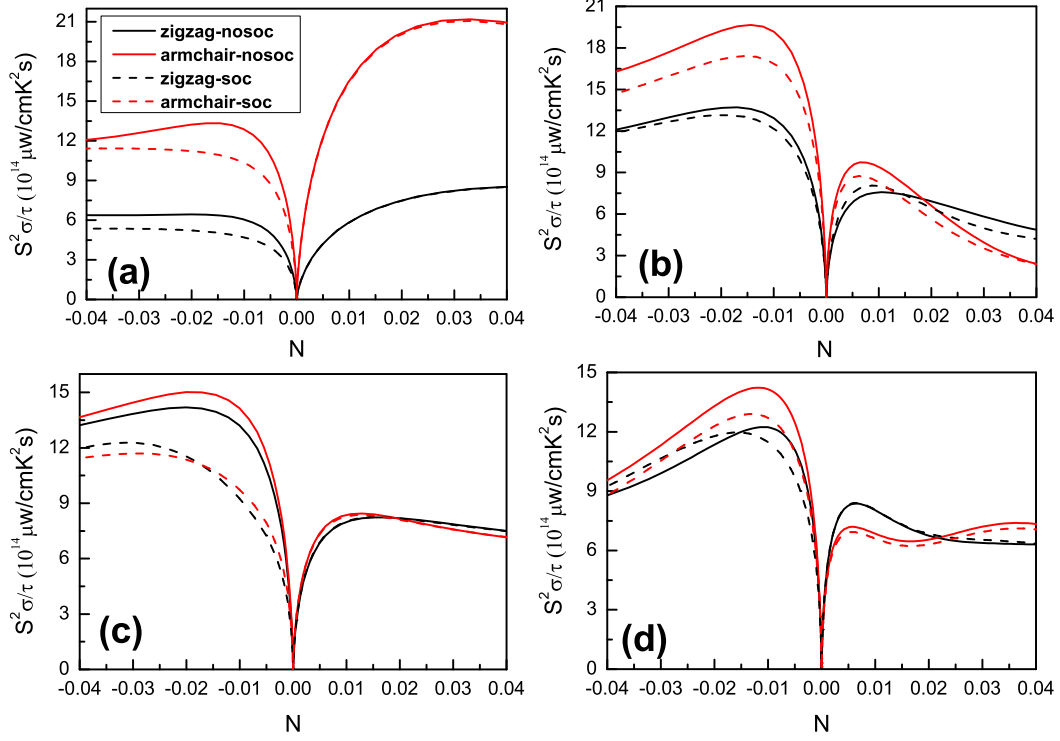


FIG. 3. (Color online) At room temperature (300 K), the power factor with respect to scattering time $S^2\sigma/\tau$ of GeS (a), GeSe (b), SnS (c) and SnSe (d) for zigzag and armchair directions as a function of doping level (N) using GGA and GGA+SOC. The doping level (N) implies electrons (minus value) or holes (positive value) per unit cell.

results, we use at least 6000 k-points in the first Brillouin zone for the self-consistent calculation, make harmonic expansion up to $l_{\max} = 10$ in each of the atomic spheres, and set $R_{\text{mt}} * k_{\max} = 8$. The self-consistent calculations are considered to be converged when the integration of the absolute charge-density difference between the input and output electron density is less than $0.0001|e|$ per formula unit, where e is the electron charge. Based on the calculated electronic energy, the semi-classic transport coefficients, such as Seebeck coefficient, electrical conductivity and electronic thermal conductivity, are performed through solving Boltzmann transport equations within the constant scattering time approximation (CSTA) as implemented in BoltzTrap³⁶ (Note: For 2D materials, the parameter LPFAC usually can not choose the default value 5, and should choose larger value. Here, we choose LPFAC value for 20.), which has been proved to be very effective for several materials^{37–39}. To obtain accurate transport coefficients, at least 22000 k-points are used in the first Brillouin zone for the energy band calculation.

III. MAIN CALCULATED RESULTS AND ANALYSIS

The orthorhombic group IV-VI monolayers AB (A=Ge and Sn; B=S and Se) possess hinge-like structure, A (B) of which is covalently bonded to three neighbors of B (A),

forming zigzag and armchair directions. The unit cell of monolayer AB (A=Ge and Sn; B=S and Se) contains two A and two B atoms, which is constructed with the vacuum region of more than 15 Å to avoid spurious interaction. The schematic crystal structure and corresponding Brillouin-zone are shown in Figure 1. The space group of monolayers AB (A=Ge and Sn; B=S and Se) is $Pmn2_1$ (No. 31), possessing lower symmetry than phosphorene with $Pmna$ (No. 53), which is due to different types of atoms constituting the compounds compared with phosphorene. The two sublayers of phosphorene are parallel to each other, but not for group IV-VI monolayers. The optimized lattice constants a and b along zigzag and armchair directions²² are used to investigate their electronic structures and thermoelectric properties, which are summarized in Table I.

Firstly, we investigate the electronic structures of group IV-VI monolayers AB (A=Ge and Sn; B=S and Se) using GGA and GGA+SOC, and show their energy band structures in Figure 2. Both GGA and GGA+SOC results show they all are indirect-gap semiconductor with the conduction band minimum (CBM) being between the G and X points and valence band maximum (VBM) being between the Y and G points (Note: For GeS, the VBM is at G point. However, this depends quite sensitively on the lattice constants. In Ref.¹⁹, the VBM is still between the Y and G points with $a=3.68$ Å and $b=4.40$ Å.). The related gaps with GGA and GGA+SOC and

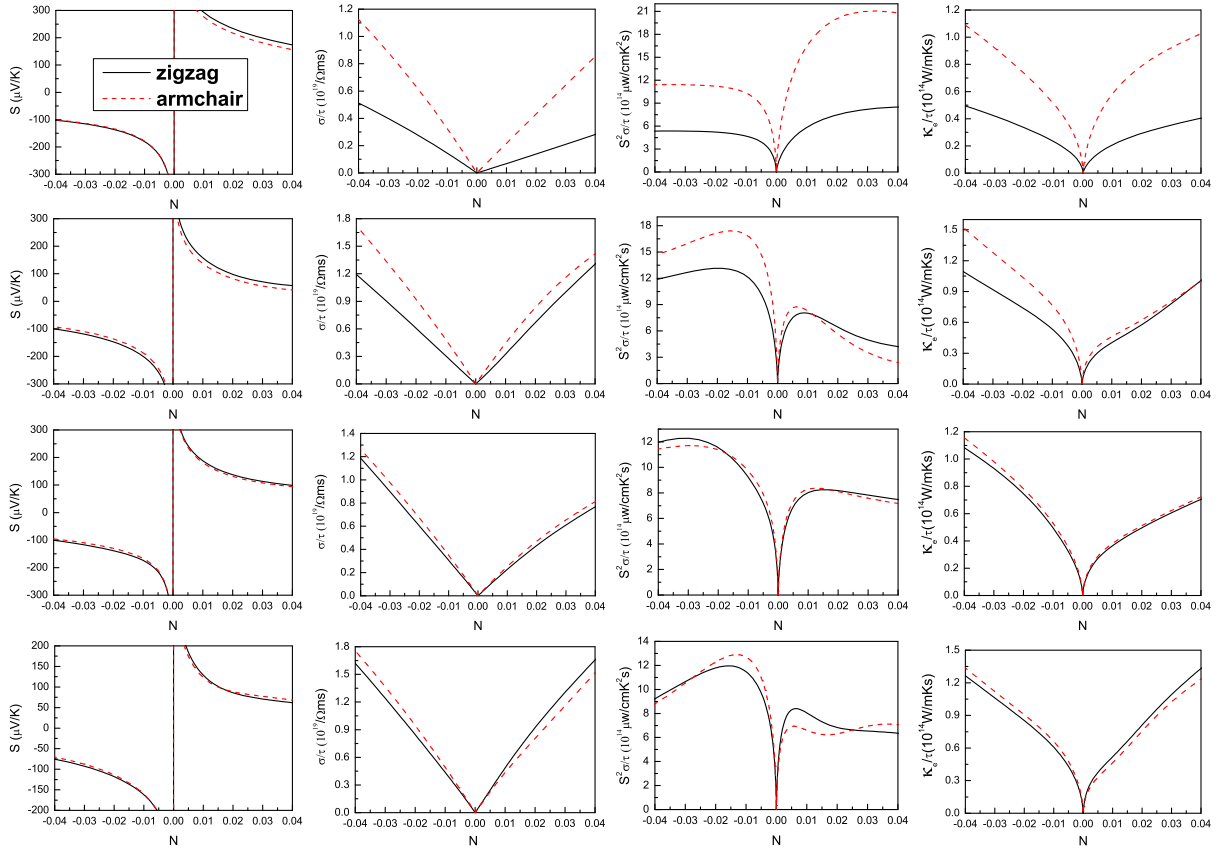


FIG. 4. (Color online) At room temperature, transport coefficients of GeS (First layer), GeSe (Second layer), SnS (Third layer) and SnSe (Fourth layer) for zigzag and armchair directions as a function of doping level (N): Seebeck coefficient S , electrical conductivity with respect to scattering time σ/τ , power factor with respect to scattering time $S^2\sigma/\tau$ and electronic thermal conductivity with respect to scattering time κ_e/τ using GGA+SOC.

the differences between them are summarized in Table I, which are consistent with previous theoretical results¹⁹. The SOC has smaller effects on group IV-VI monolayers than transition-metal dichalcogenide monolayers¹⁰, and the representative spin-orbit splitting values at the CBM are listed in Table I, which are in agreement with previous theoretical values¹⁹. Among group IV-VI monolayers, the SOC produces the largest effects on valence bands near the Fermi level for SnS, which will lead to obvious influences on p-type power factor of SnS. According to their energy band structures, it is found that the symmetry along G-X-S and G-Y-S directions gradually increases from GeS to SnSe, which is because the difference between a along zigzag direction and b along armchair direction gradually decreases. The smaller difference leads to less anisotropic thermoelectric properties. The conduction and valence bands near the Fermi level also show a certain symmetry, especially for SnS and SnSe.

The SOC has very important influences on electronic transport coefficients in many thermoelectric materials^{9,10,23-28}. Here, we firstly consider SOC effects on transport coefficients of group IV-VI monolayers. On the basis of energy band structure with GGA

and GGA+SOC, the semi-classic transport coefficients, including Seebeck coefficient S and electrical conductivity with respect to scattering time σ/τ , are calculated within CSTA Boltzmann theory. The rigid band approach is employed, which is reasonable, if the doping level is low⁴⁰⁻⁴². The doping effects are mimicked by shifting the Fermi level. The power factor with respect to scattering time $S^2\sigma/\tau$ along zigzag and armchair directions as a function of doping level (N) at room temperature using GGA and GGA+SOC are shown in Figure 3. Calculated results show that SOC has obvious detrimental effects on power factor in n-type doping for GeS and SnS, while has negligible influences for p-type. For GeSe and SnSe, the power factor along armchair direction with GGA+SOC is reduced compared to one with GGA, while slightly improved effect is observed along zigzag direction. These can be understood by considering SOC effects on the conduction or valence bands near the Fermi level. The SOC can remove the band degeneracy by spin-orbit splitting, leading to reduced S , and gives rise to reduced power factor. However, SOC-removed band degeneracy also can make two band extrema to be more close, which can induce improved S , and then enhances power factor. Similar SOC effects on power fac-

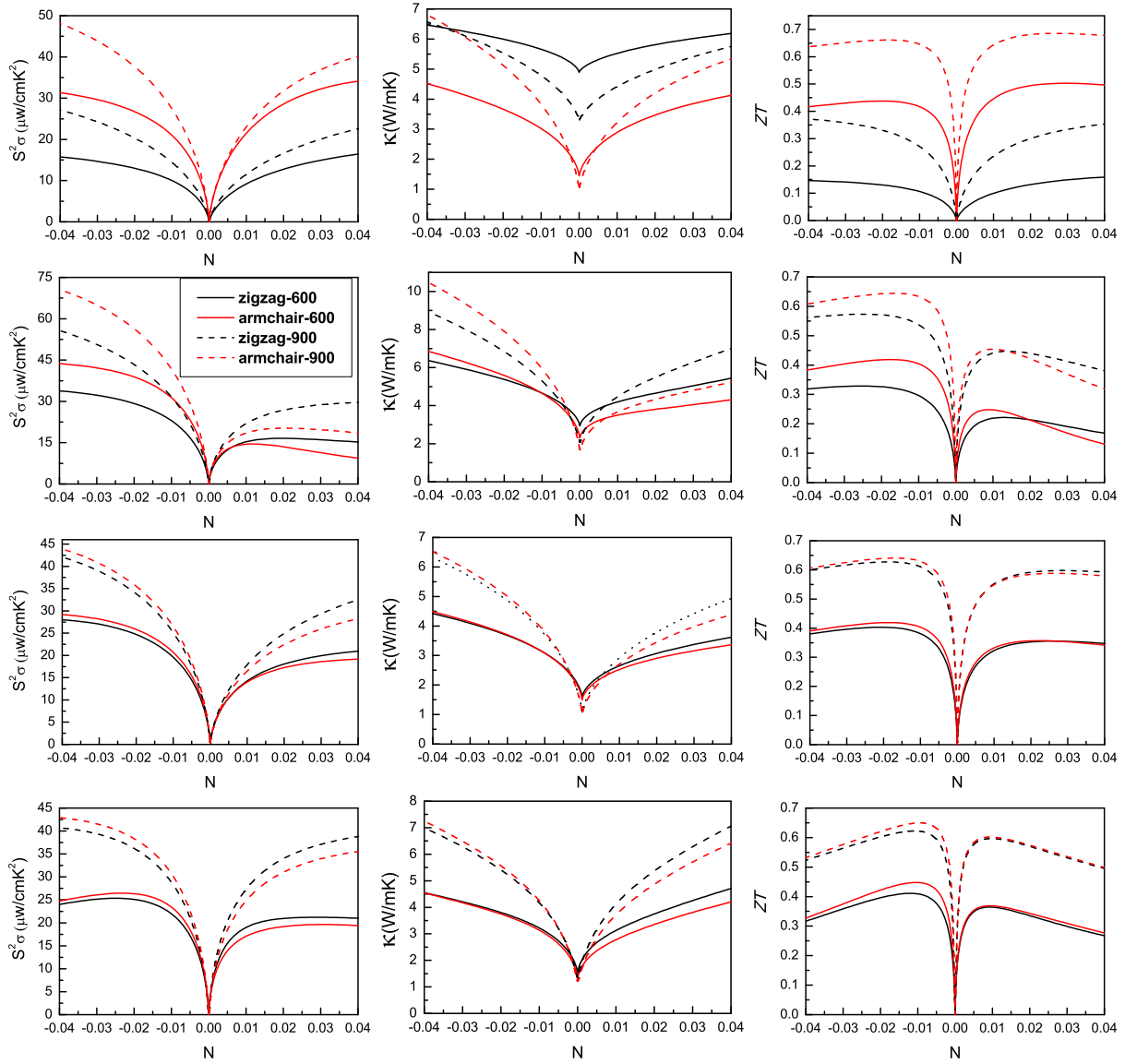


FIG. 5. (Color online) At 600 K and 900 K, the power factor $S^2\sigma$, total thermal conductivity κ and ZT of GeS (First layer), GeSe (Second layer), SnS (Third layer) and SnSe (Fourth layer) for zigzag and armchair directions as a function of doping level with the scattering time τ being 1×10^{-14} s.

tor can also be found in semiconducting transition-metal dichalcogenide monolayers^{9,10}. For SnS, the maximum power factors along zigzag and armchair directions at 300 K with SOC are predicted to be about 13.47% and 22.07% smaller than those without SOC in the case of n-type doping. Therefore, it is necessary to consider SOC effects for theoretical analysis of thermoelectric properties in group IV-VI monolayers.

Next, room-temperature transport coefficients of group IV-VI monolayers AB (A=Ge and Sn; B=S and Se) for zigzag and armchair directions as a function of doping level, including Seebeck coefficient S , electrical conductivity with respect to scattering time σ/τ , power factor with respect to scattering time $S^2\sigma/\tau$ and electronic thermal conductivity with respect to scattering

time κ_e/τ , are plotted in Figure 4 within GGA+SOC. In n-type doping, the anisotropy of thermoelectric transport coefficients along zigzag and armchair directions is very obvious for GeS and GeSe, while only anisotropy of GeS is very remarkable in p-type doping. These can be explained by their feature of energy band structure. The profile of energy bands along G-X-S and G-Y-S directions for GeS and GeSe has weaker symmetry than one of SnS and SnSe. It is found that n-type doping has more better power factor than p-type one for GeSe, SnS and SnSe, while it is opposite for GeS. Another notable thing is that the GeS along armchair direction in p-type doping shows highest power factor, which can be explained by band convergence¹. The valence band extrema (VBE) along Y-G and at G point are very close,

and the energy difference only is 0.007 eV, which leads to large S , inducing high power factor. The electronic thermal conductivity has similar outlines with electrical conductivity, which is because that the electrical thermal conductivity is connected with electrical conductivity by the Wiedemann-Franz law: $\kappa_e = L\sigma T$, where L is the Lorenz number.

Finally, the figure of merit ZT is calculated to estimate the efficiency of thermoelectric conversion, which needs scattering time τ and lattice thermal conductivity κ_L . It is challenging to calculate scattering time τ from the first-principle calculations because of the complexity of various carrier scattering mechanisms. Here, a typical $\tau = 10^{-14}$ s is used to attain power factor and electrical thermal conductivity (In Ref.¹¹, this value is also adopted in the thermoelectric calculations of bulk orthorhombic IV-VI compounds.). In Ref.²², the lattice thermal conductivities of group IV-VI monolayers AB (A=Ge and Sn; B=S and Se) have been investigated in detail. The lattice thermal conductivities along the zigzag and armchair directions show the strongest anisotropy for GeS, while the ones of monolayer SnS and SnSe are very weak, which is similar with electron transport. The lattice thermal conductivities of four monolayers all almost go as $1/T$ at medium temperatures. The lattice thermal conductivities of group IV-VI monolayers along zigzag and armchair directions at 600 and 900 K are attained from room-temperature ones. At 600 K and 900 K, the power factor $S^2\sigma$, total thermal conductivity κ and ZT of group IV-VI monolayers AB (A=Ge and Sn; B=S and Se) for zigzag and armchair directions as a function of doping level with the scattering time τ being 1×10^{-14} s are plotted in Figure 5. It is found that the anisotropic behavior of ZT is keeping pace with that of power factor, electronic and lattice thermal conductivity. For GeS and n-type GeSe, the ZT along armchair direction is much larger than one along zigzag direction. The ZT values along zigzag and armchair directions of p-type GeSe, SnS and SnSe show less anisotropic behavior, especially for SnS. Another interesting thing is that n- and p-type ZT values of GeS, SnS and SnSe show little difference. For GeSe, n-type doping shows better thermoelectric performance than p-type one. According to their average ZT along zigzag and armchair directions, it is clearly shown that n-type GeSe, SnS and SnSe exhibit almost excellent thermoelectric performance, while GeS and p-type GeSe have relatively weak one.

IV. DISCUSSIONS AND CONCLUSION

Compared to transition-metal dichalcogenide monolayers, the SOC has rather little effect on electronic structures of orthorhombic group IV-VI monolayers. The spin-orbit splitting of transition-metal dichalcogenide monolayers at representative point is 0.09 eV \sim 0.49 eV^{9,10}, which is larger than that of group IV-VI monolayers from 0.046 eV to 0.099 eV except for ZrS₂ (0.09 eV).

However, SOC can induce observable influence on power factor of group IV-VI monolayers, especially for n-type SnS due to the largest spin-orbit splitting at CBM. Both reduced and enhanced effects on power factor induced by SOC are found in group IV-VI monolayers, which is similar with transition-metal dichalcogenide monolayers^{9,10}. Unlike bulk Mg₂Sn²⁴ and half-Heusler ANiB (A=Ti, Hf, Sc, Y; B=Sn, Sb, Bi)²⁵, only detrimental influences on power factor are observed. So, it is necessary for electron transport of group IV-VI monolayers to include SOC.

The electronic structure of 2D materials is quite sensitive to strain, which can induce band convergence, further enhancing thermoelectric properties. Group IV-VI monolayers have some VBE and conduction band extrema (CBE) near the Fermi level, and their relative positions of energy level can be tuned by strain. For monolayer SnSe, Both CBE and VBE along G-X or G-Y and at G point can approach each other by strain⁴³, which can achieve band convergence, improving power factor¹. In fact, the band convergence can be observed in GeS with $a=3.671$ Å and $b=4.457$ Å used in the work, and the VBE along G-Y and at G point almost coincide, exhibiting high power factor. However, if the lattice constants $a=3.68$ Å and $b=4.40$ Å in Ref.¹⁹ are used, the band convergence should not occur. Similar strain-induced band convergence also can be found in transition-metal dichalcogenide monolayer MoS₂⁹. So, it is possible to tune thermoelectric properties of group IV-VI monolayers by strain.

If we assume that the scattering time is fixed, group IV-VI monolayers have more higher power factor than semiconducting transition-metal dichalcogenide monolayers MX₂ (M=Zr, Hf, Mo, W and Pt; X=S, Se and Te) expect for PtX₂ (X=S, Se and Te) at 300 K, which can be easily observed from Figure 4 and Figure 5 in Ref.¹⁰. They have more lower lattice thermal conductivities than transition-metal dichalcogenide monolayers like MS₂ and MSe₂ (M=Zr, Hf, Mo and W)⁴⁴. The average lattice thermal conductivities along the zigzag and armchair directions of GeS (6.38), GeSe (5.23), SnS (3.08) and SnSe (2.77) all are lower than that of MoS₂ (103.4), WS₂ (141.9), MoSe₂ (54.21), WSe₂ (52.47), ZrS₂ (13.31), HfSe₂ (11.30), HfS₂ (16.56) and ZrSe₂ (10.10) [The unit of thermal conductivity: Wm⁻¹K⁻¹]. Therefore, group IV-VI monolayers may be potential 2D thermoelectric materials.

In summary, the first-principles combined with the Boltzmann transport theory are used to investigate the thermoelectric properties of orthorhombic group IV-VI monolayers AB (A=Ge and Sn; B=S and Se), and the SOC is also included for electron transport. Although the SOC influences on electronic structures are not very obvious, SOC-induced splitting produces observable effects on power factor. The four monolayers show diverse anisotropic thermoelectric properties, and GeS along the zigzag and armchair directions shows the strongest anisotropy while SnS and SnSe show an almost isotropy. In n-type doping, it is found that four monolayers show

similar efficiency of thermoelectric conversion along armchair direction, and GeS shows the weakest one along zigzag direction compared with GeSn, SnS and SnSe. For p-type, GeSe shows the lowest ZT along armchair direction, and GeS and GeSe exhibit weaker conversion efficiency along zigzag direction. The present work will further stimulate experimental studies of 2D high-efficient thermoelectric materials.

ACKNOWLEDGMENTS

This work is supported by the Fundamental Research Funds for the Central Universities (2015XKMS073). We are grateful to the Advanced Analysis and Computation Center of CUMT for the award of CPU hours to accomplish this work.

- ¹ Y. Pei, X. Shi, A. LaLonde, H. Wang, L. Chen and G. J. Snyder, *Nature* **473**, 66 (2011).
- ² L. E. Bell, *Science* **321**, 1457 (2008).
- ³ M. S. Dresselhaus et al. *Adv. Mater.* **19**, 1043 (2007).
- ⁴ R. Fei, A. Faghaninia, R. Soklaski, J. A. Yan, C. Lo and L. Yang, *Nano Lett.* **14**, 6393 (2014).
- ⁵ K. Yang, S. Cahangirov, A. Cantarero, A. Rubio and R. D'Agosta, *Phys. Rev. B* **89**, 125403 (2014).
- ⁶ J. Wu et al. *Nano Lett.* **14**, 2730 (2014).
- ⁷ Z. Jin et al. *Sci. Rep.* **5**, 18342 (2015).
- ⁸ S. Kumar and U. Schwingenschlögl, *Chem. Mater.* **27**, 1278 (2015).
- ⁹ S. D. Guo, *Comp. Mater. Sci.* **123**, 8 (2016).
- ¹⁰ S. D. Guo and J. L. Wang, *Semicond. Sci. Tech.* in press.
- ¹¹ G. Ding, G. Gao and K. Yao, *Sci. Rep.* **5**, 9567 (2015).
- ¹² L. D. Zhao, S. H. Lo, Y. Zhang, H. Sun, G. Tan, C. Uher, C. Wolverton, V. P. Dravid and M. G. Kanatzidis, *Nature* **508**, 373 (2014).
- ¹³ L. D. Zhao, G. Tan, S. Hao, J. He, Y. Pei, H. Chi, H. Wang, S. Gong, H. Xu and V. P. Dravid, *Science* **351**, 141 (2016).
- ¹⁴ L. Li, Z. Chen, Y. Hu, X. Wang, T. Zhang, W. Chen and Q. Wang, *J. Am. Chem. Soc.* **135**, 1213 (2013).
- ¹⁵ F. Q. Wang, S. Zhang, J. Yu and Q. Wang, *Nanoscale* **7**, 15962 (2015).
- ¹⁶ L. C. Zhang, G. Qin, W. Z. Fang, H. J. Cui, Q. R. Zheng, Q. B. Yan and G. Su, *Sci. Rep.* **6**, 19830 (2016).
- ¹⁷ G. Ding, G. Gao et al., arXiv preprint arXiv:1509.01759, 2015.
- ¹⁸ W. J. Baumgardner, J. J. Choi, Y.-F. Lim and T. Hanrath, *J. Am. Chem. Soc.* **132**, 9519 (2010).
- ¹⁹ L. C. Gomes and A. Carvalho, *Phys. Rev. B* **92**, 085406 (2015).
- ²⁰ R. Fei, W. Li, J. Li and L. Yang, *Appl. Phys. Lett.* **107**, 173104 (2015).
- ²¹ M. H. Wu and X. C. Zeng, *Nano Lett.* **16**, 3236 (2016).
- ²² G. Qin, Z. Qin, W. Fang, L. Zhang, S. Yue, Q. Yan, M. Hu and G. Su, *Nanoscale* **16**, 3236 (2016).
- ²³ K. Kutorasinski, B. Wiendlocha, J. Tobola and S. Kaprzyk, *Phys. Rev. B* **89**, 115205 (2014).
- ²⁴ S. D. Guo and J. L. Wang, *RSC Adv.* **6**, 31272 (2016).
- ²⁵ S. D. Guo, *J. Alloy. Compd.* **663**, 128 (2016).
- ²⁶ P. Larson, S. D. Mahanti, and M. G. Kanatzidis, *Phys. Rev. B* **61**, 8162 (2000).
- ²⁷ T. J. Scheidemantel, C. Ambrosch-Draxl, T. Thonhauser, J. V. Badding, and J. O. Sofo, *Phys. Rev. B* **68**, 125210 (2003).
- ²⁸ S. J. Youn and A. J. Freeman, *Phys. Rev. B* **63**, 085112 (2001).
- ²⁹ P. Hohenberg and W. Kohn, *Phys. Rev.* **136**, B864 (1964); W. Kohn and L. J. Sham, *Phys. Rev.* **140**, A1133 (1965).
- ³⁰ P. Blaha, K. Schwarz, G. K. H. Madsen, D. Kvasnicka and J. Luitz, WIEN2k, an Augmented Plane Wave + Local Orbitals Program for Calculating Crystal Properties (Karlheinz Schwarz Technische Universität Wien, Austria) 2001, ISBN 3-9501031-1-2
- ³¹ J. P. Perdew, K. Burke and M. Ernzerhof, *Phys. Rev. Lett.* **77**, 3865 (1996).
- ³² A. H. MacDonald, W. E. Pickett and D. D. Koelling, *J. Phys. C* **13**, 2675 (1980).
- ³³ D. J. Singh and L. Nordstrom, *Plane Waves, Pseudopotentials and the LAPW Method*, 2nd Edition (Springer, New York, 2006).
- ³⁴ J. Kunes, P. Novak, R. Schmid, P. Blaha and K. Schwarz, *Phys. Rev. B* **64**, 153102 (2001).
- ³⁵ D. D. Koelling, B. N. Harmon, *J. Phys. C: Solid State Phys.* **10**, 3107 (1977).
- ³⁶ G. K. H. Madsen and D. J. Singh, *Comput. Phys. Commun.* **175**, 67 (2006).
- ³⁷ B. L. Huang and M. Kaviani, *Phys. Rev. B* **77**, 125209 (2008).
- ³⁸ L. Q. Xu, Y. P. Zheng and J. C. Zheng, *Phys. Rev. B* **82**, 195102 (2010).
- ³⁹ J. J. Pulikkotil, D. J. Singh, S. Auluck, M. Saravanan, D. K. Misra, A. Dhar and R. C. Budhani, *Phys. Rev. B* **86**, 155204 (2012).
- ⁴⁰ T. J. Scheidemantel, C. Ambrosch-Draxl, T. Thonhauser, J. V. Badding and J. O. Sofo, *Phys. Rev. B* **68**, 125210 (2003).
- ⁴¹ G. K. H. Madsen, *J. Am. Chem. Soc.* **128**, 12140 (2006).
- ⁴² X. Gao, K. Uehara, D. Klug, S. Patchkovskii, J. Tse and T. Tritt, *Phys. Rev. B* **72**, 125202 (2005).
- ⁴³ L. C. Zhang et al. *Sci. Rep.* **6**, 19830 (2016).
- ⁴⁴ X. K. Gu and R. G. Yang, *Appl. Phys. Lett.* **105**, 131903 (2014).